Mat. Res. Soc. Symp. Proc. Vol. 675 © 2001 Materials Research Society

A MODEL TO INTERPRET THE RAMAN SPECTRA OF DISORDERED, AMORPHOUS AND NANOSTRUCTURED CARBONS

Andrea Carlo Ferrari
Department of Engineering, University of Cambridge, Cambridge, CB2 1PZ, UK

ABSTRACT

Raman spectroscopy is a very popular, non-destructive tool for the structural characterisation of carbons. Raman scattering from carbons is always a resonant process, in which those configurations whose band gaps match the excitation energy are preferentially excited. The Raman spectra of carbons do not follow the vibration density of states, but consist of three basic features, the G and D peaks around 1600 and 1350 cm^{-1} and an extra T peak, for UV excitation, at ~980-1060 cm^{-1}. The Raman spectra at any wavelength depend on 1) clustering of the sp^2 phase, 2) bond length and bond angle disorder, 3) presence of sp^2 rings or chains, and 4) the sp^2/sp^3 ratio. It will be shown how the basic features of the Raman spectra vary by rationalising them within a three-stage model of order of carbons. It is shown how the three-stage model can account for the vast range of experimental data available for Raman experiments at any excitation wavelength. This model can also account for apparently contradictory trends reported in literature, since the clustering of the sp^2 phase and the sp^3 to sp^2 conversion are separately treated.

INTRODUCTION

Carbon is unique in the way that simple changes in its local bonding can give rise materials as diverse as diamond, graphite, fullerenes, carbon nanotubes, and disordered, nano-structured and amorphous carbons. These materials have a remarkable range of mechanical, electronic and electrochemical properties and many possible applications [1,2]. It is thus very useful to develop fast, reliable, non-destructive techniques to probe the key parameters which control their physical behaviour.

We are particularly interested in amorphous carbons. We define diamond-like carbon (DLC) as an amorphous carbon (a-C) or an hydrogenated amorphous carbon (a-C:H) with a significant fraction of sp^3 bonds. A-C:H often has a rather small C-C sp^3 content. DLC's with highest sp^3 content (80-90%) are called tetrahedral amorphous carbon (ta-C) and its hydrogenated analogue ta-C:H. The key parameters of interest in such materials are: 1) the sp^3 content; 2) the clustering of the sp^2 phase; 3) the orientation or anisotropy of the sp^2 phase; 4) any cross sectional structure; 5) the H content. The sp^3 content alone mainly controls the elastic constants, but films with the same sp^3 and H content but different sp^2 clustering, sp^2 orientation or cross-sectional nano-structure can have different optical, electronic and mechanical properties.

Raman spectroscopy is a popular, non-destructive tool for structural characterisation of carbons [3-12]. It is traditionally carried out at the commonly available wavelengths in the blue-green spectral region (488-514.5 nm), but multi-wavelength Raman (MW Raman) studies are becoming increasingly used. Indeed, Raman scattering from carbons is always a resonant process, in which configurations whose band gaps match the excitation energy are preferentially excited. Any mixture of sp^3, sp^2 and sp^1 carbon atoms always has a gap between 0 and 5.5 eV, and this energy range matches that of IR-vis-UV Raman systems. This implies that understanding the resonant Raman process in carbon systems will give a powerful, fast means for their structural and electronic characterisation. For example, MW Raman has recently been used to distinguish the metallic and semiconducting forms of single

wall carbon nanotubes [10,11]. It has also been used to investigate the origin of the peaks at ~1150 cm^{-1} and ~1450 cm^{-1} in nano-crystalline diamond [13].

The Raman spectra of all carbons show several common features in the 800-2000 cm^{-1} region, the so-called G and D peaks, which lie at around 1560, 1360 cm^{-1} for visible excitation, and the T peak, seen for UV excitation at around 1060 cm^{-1}. The G and D peaks are due to sp^2 sites only. The G peak is due to the bond stretching of all pairs of sp^2 atoms in both rings and chains [7]. The D peak is due to the breathing modes of sp^2 atoms in rings. The T peak is due to the C-C sp^3 vibrations and appears only in UV excitation.

Although Raman spectroscopy of carbons has continued for 30 years, there have been significant advances in our understanding recently. Firstly, C-C sp^3 vibrations were directly detected using UV Raman spectroscopy at 244nm [14-16]. The second major advance is the understanding of the origin of the D peak. Pocsik et al. [17] and others [18,19] proposed empirically that the D peak arises as a resonant Raman coupling to the phonon of wave vector q when it equals the wave vector k of the electronic transition excited by the incident phonon. We called this a k=q "quasi selection rule", since it qualitatively explains the observed trends, but the physical mechanism behind the resonance was not fully understood [7]. Recently, Thomsen and Reich [20] showed how the D peak arises from a double resonant Raman process. For a particular excitation energy E, an electron-hole pair is created at the k point matching the energy gap between the conduction and valence band. The electron is then scattered across the zone by a phonon ω(q), this being the phonon for which the double resonance occurs. The electron is then scattered back elastically by lattice defects or disorder and recombines with the hole, conserving k in the process. It can be seen that this double resonance occurs when [20, 12]:

$$k \approx \tfrac{1}{2} q \qquad (1)$$

rather than the k≈q originally heuristically proposed [17,18,7]. This, in contrast to what stated in ref.[20], does not affect our conclusions on the nature of the D peak and on which optical branch contributes to the peak [7]. It generalises the concept of L_a in case of graphite to being an inter-defect distance.

For disordered carbons, one can map the energy levels and vibration modes of carbon clusters onto those of graphite [7]:

$$1/L_a \Leftrightarrow k \text{ and } 1/L_a \Leftrightarrow q \qquad (2)$$

where L_a is the cluster size or in plane correlation length. (2) is the basis to explain the origin and dispersion of the D peak in disordered and amorphous carbons and to derive the real space motions (breathing modes) of the phonons giving rise to this band [7,21,22]. We could thus propose a three-stage model to relate the visible Raman spectra of disordered and amorphous carbons to their local bonding [7].

Mapelli et al.[21,22] showed that the breathing motions of clusters of increasing size could be mapped on the upper optical branch of the graphite dispersion relations from K to (K-M)/2, with q=(K-M)/2=π/(3a)~1.05/a corresponding to coronene. In graphitic clusters, the π states have minimum band energies of roughly [1,7]:

$$E_g \approx \frac{2\gamma}{M^{0.5}} \approx 2\gamma \frac{a}{L_a} \qquad (3)$$

where M is the number of aromatic rings in the cluster and L_a is the cluster diameter. For example, coronene is composed of 7 rings, and from (3) we can estimate its optical gap as $6/\sqrt{7}$ eV. This corresponds to the gap of graphite at k=$2/\sqrt{21}$ a~0.44/a [12]. Thus eq. (1) links breathing modes of clusters, and thus L_a, with k and q. This implies that, for all modes satisfying the double resonance condition, the breathing modes on the upper optical branch are enhanced due to their high polarizability. This allows a unified interpretation of the origin

of the D peak in amorphous carbons and polycyclic aromatic hydrocarbons, due to the mapping of the electronic and vibrational states of carbon clusters onto those of graphite.

We show that the peak dispersions in a-C, ta-C, ta-C:H, diamond-like a-C:H and polymeric a-C:H can be considered as canonical cases in the ternary phase diagram of the disordered C:H system [7,1]. We propose a general explanation of the trends in peak positions and intensities, and extend the previous 3-stage model [7] to spectra excited at many wavelengths [12]. A main conclusion is that the spectra and their dispersion are characteristic of each type of carbon, while their single wavelength Raman spectrum may be indistinguishable. We then show how a simpler 2-wavelength (visible-UV) study can provide most of the information on the fraction and order of sp^2 sites in amorphous carbons.

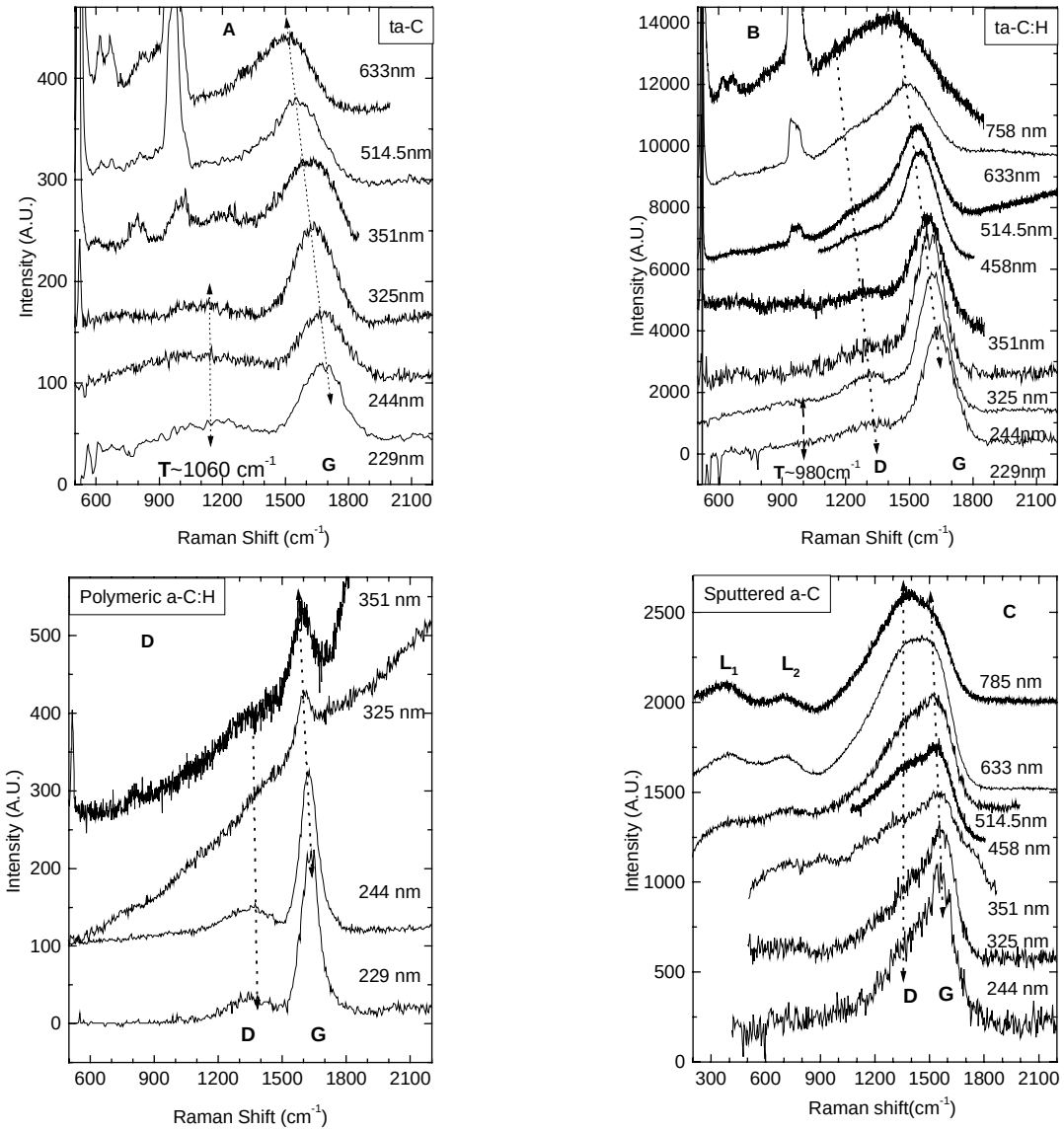

Fig 1: Multi-wavelength Raman spectra of (A) ta-C, (B) ta-C:H, (C) sputtered a-C and (D) polymeric a-C:H. The peaks' trends and labels are indicated. Two extra peaks at ~400 and 800 cm^{-1} are seen in the sputtered a-C; these are typical of low sp^3 a-C and are not discussed here.

EXPERIMENTAL

Unpolarised Raman spectra were acquired at λ=229, 244, 325, 351, 458, 514.5, 532, 633, 785 nm (5.41-1.58 eV) using a variety of spectrometers. The power on the sample was

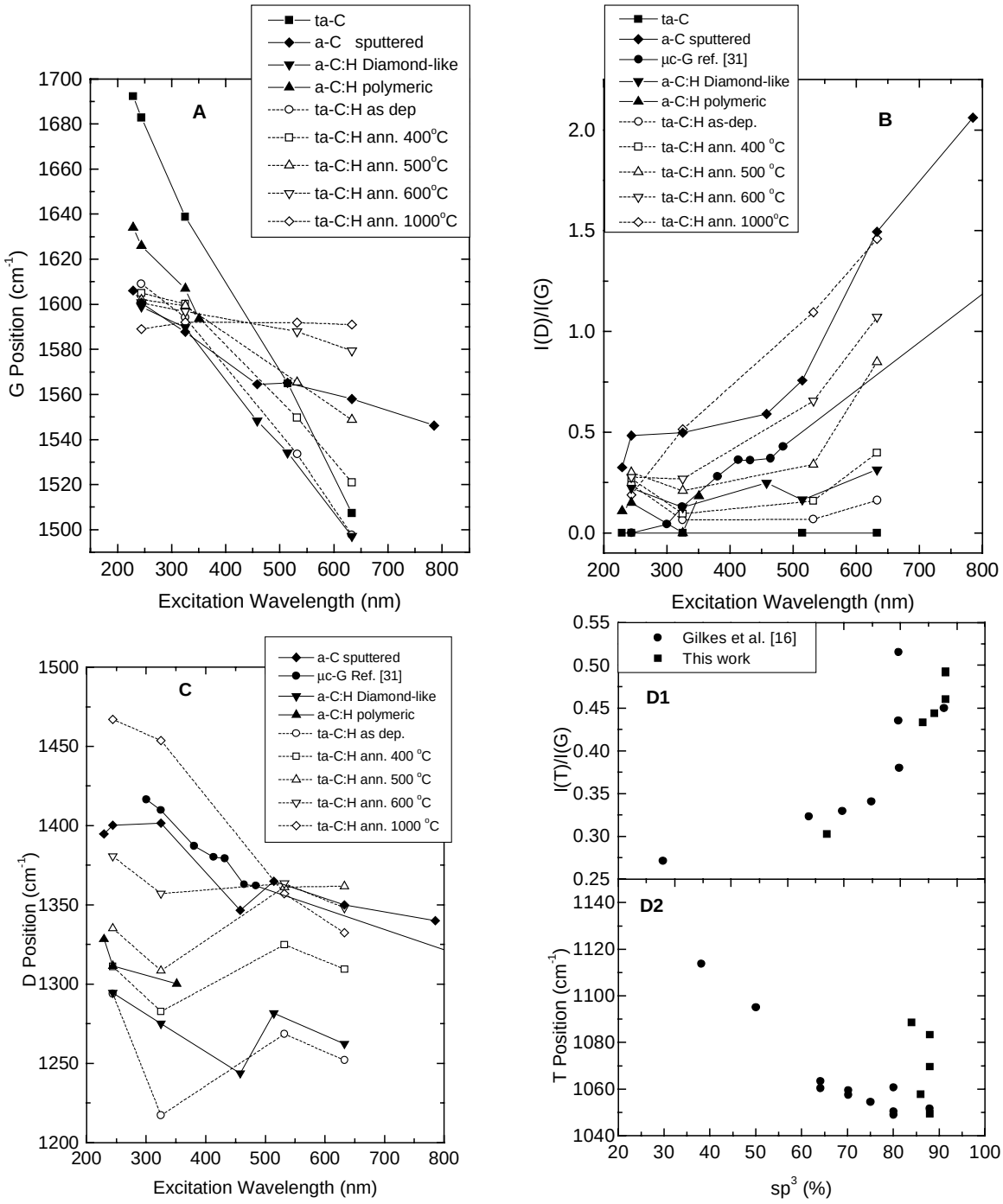

Fig.2: A,B,C) Dispersion of G peak, I(D)/I(G) and D peak vs. excitation wavelength for a series of template samples; (D1,D2) I(T)/I(G) and T peak position vs. sp^3 fraction for non hydrogenated carbon films. Note that data on a series of annealed ta-C:H, on diamond-like a-C:H and on micro crystalline graphite are also shown. 600 ^{0}C is the onset of major H effusion and sp^3 to sp^2 conversion in ta-C:H [23,24]

kept well below 1mW. Sample damage is always an issue in Raman measurements, but it is particularly serious for UV excitation. For H containing samples, in order to be sure that the signal we measured is a genuine feature of a-C:H samples, we performed measurements with samples rotating at a very high speed (>3000 rpm) with a random XY movement superimposed. We have analysed a variety of carbon samples. As we focus on general trends, we discuss only selected cases. Fig 1 shows the multi-wavelength Raman spectra of ta-C, ta-C:H, a-C and polymeric a-C:H samples [12].

The spectra in general show three features, around 1560, 1360 (for visible excitation) and 1060 cm^{-1} (detected only in UV excitation), which are labelled as the G, D and T peaks, respectively. The G and D peaks are due to sp^2 sites only. The G peak is due to the bond stretching of all pairs of sp^2 atoms in both rings and chains [7]. The D peak is due to the breathing modes of rings. The T peak is due to C-C sp^3 vibrations and appears only for UV excitation. The trends in the D, G and T peaks are indicated in Fig 2.

For visible excitation, the sp^2 sites have such a high cross-section that they dominate the spectra, the sp^3 sites are invisible and the spectrum responds only to the configuration or order of the sp^2 sites. As the excitation energy rises, two effects occur, resonance causes the excitation of those sp^2 configurations with a wider gap, and then in the deep UV the modes of σ states of C-C bonds are seen.

TRENDS IN RAMAN PARAMETERS

Three stage model

The trends in the Raman parameters for different laser excitation can be rationalised by extending the three-stage model that we proposed to explain the trends in visible Raman spectra [7]. This model considers an amorphisation trajectory, consisting of three stages from graphite to ta-C (or diamond):

1) graphite→nanocrystalline graphite (nc-G)
2) nanocrystalline graphite→ sp^2 a-C
3) a-C→ta-C (→ 100 sp^3 ta-C, defected diamond),

Broadly, stage 1 corresponds to the reduction of the in-plane correlation length L_a within an ordered graphite layer. Stage 2 is the introduction of topological disorder into the graphite layer. Stage 3 is the conversion of sp^2 sites to sp^3 sites and the consequent change of sp^2 configuration from rings to chains.

The Raman spectra depend on

1) clustering of the sp^2 phase
2) bond length and bond angle disorder
3) presence of sp^2 rings or chains
4) the sp^2/sp^3 ratio

We note that any features above ~1360 cm^{-1} cannot be due to C-C sp^3 vibrations, being this the band limit for C-C sp^3 vibrations [7]. Thus, it is clear that the presence of G peaks in Fig 1 means that sp^2 vibrations still dominate even in the UV Raman excitation. In the following sections we will discuss the G, D and T peaks, extending the 3-stage model to multi-wavelength excitation.

The G peak

Fig 2(A) shows the variation of the position of the G peak with excitation wavelength and energy. The G peak does not disperse in graphite itself, nanocrystalline (nc)-graphite or glassy carbon [25, 29-31]. The G peak only disperses in more disordered carbon, where the dispersion is proportional to the degree of disorder. This is an important finding, by which the physical behaviour of the G peak in disordered graphite is radically different from amorphous carbons, even though the G peak positions might accidentally be the same at

some excitation energy. The G peak in graphite cannot disperse because it is the Raman-active phonon mode of the crystal. In nc-graphite, the G peak shifts slightly upwards at fixed excitation energy due to phonon confinement, but it cannot disperse with varying excitation energy, still being a density of states feature. The G peak dispersion occurs only in more disordered carbon, because now there are a range of configurations with different local band gaps and different phonon modes. The dispersion arises from a resonant selection of sp^2 configurations or clusters with wider π band gaps, and correspondingly higher vibration frequencies. The G peak dispersion separates the materials into two types. In materials with only sp^2 rings, the G peak dispersion saturates at a maximum of ~1600 cm^{-1}, the G position in nc-graphite. In contrast, in those materials also containing sp^2 chains, particularly ta-C and ta-C:H, the G peak continues to rise past 1600 cm^{-1} and can reach 1690 cm^{-1} at 229 nm

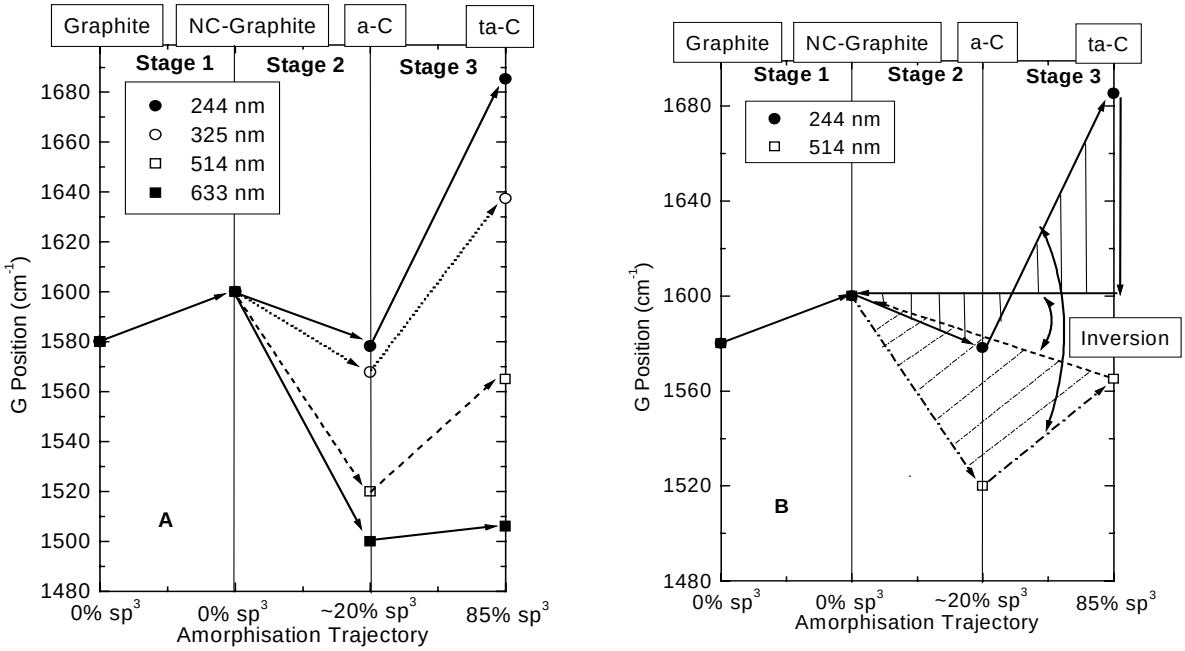

Fig 3: (A) Amorphisation trajectory, showing the schematic variation of G peak position for four typical wavelengths; (B) Amorphisation trajectory, showing the possibility of hysteresis in stages 2 and 3 for two typical wavelengths (514.5 and 244 nm). The regions span by hysteresis at 514.5 nm and 244 nm are evidenced by lines. Note the different shape of the hysteresis region for UV excitation: an inversion of the trends happens, with the highest shift Vis->UV for samples having the least ordered sp^2 phase.

excitation in ta-C. This high G peak position can only be due to short, strained C=C bonded chains, if one notes that the C=C stretching vibration in ethylene is at ~1630 cm^{-1}.

This range of behaviours of the G peak can be understood within the three-stage model of Raman spectra [7]. This plots the G mode against an *amophorisation* trajectory. The model is extended to show the variation of G position with excitation wavelength, as shown in Fig. 3 (A) for four typical wavelengths. In ref [7] we pointed out that following the reverse, *ordering* trajectory, from ta-C to graphite (by high temperature deposition, annealing after deposition, or low-dose ion implantation) there is hysteresis [7]. This means that there can be sp^2 clustering or π electron delocalisation without a corresponding $sp^2 \rightarrow sp^3$ conversion. For visible excitation, sp^2 clustering and ordering will always *raise* the G peak in stages 2 and 3. In contrast, in UV excitation, increasing clustering *lowers* the G position, as noted above. This is shown schematically in Fig 3(B). Comparing visible to UV excitation, there is an *inversion* of the trends. This is another remarkable result, since it allows for a

distinction of samples which, although having different structures, may accidentally show very similar Raman spectra at a certain wavelength.

The D peak and I(D)/I(G)

The D peak arises from the breathing motion of sp^2 rings. I(D)/I(G) is highest for IR excitation, and it decreases strongly at higher excitation energy. Although there is no D peak in the UV Raman for nc-graphite, Fig 1 suggest that there is some residual intensity in the D region in UV Raman in the more disordered carbons, those with stage 2 disorder.

Fig 2(B,C) plot the I(D)/I(G) intensity ratio and the D peak position as a function of excitation wavelength. In contrast to the G peak dispersion, the I(D)/I(G) ratio and the D peak have maximum dispersion for micro and nano-crystalline graphite, and the dispersion decreases for increasing disorder, i.e. the dispersion is proportional to order.

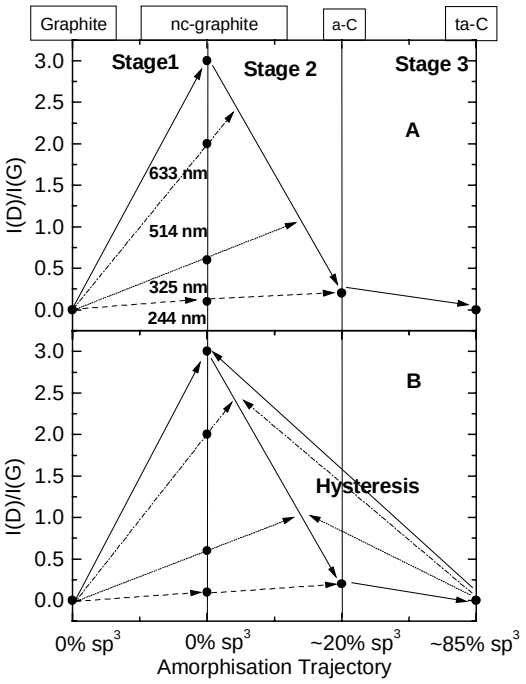

Fig 4: (A) Amorphisation trajectory, showing the schematic variation of I(D)/I(G) for four typical wavelengths. Note that for increasing excitation energy the maximum of I(D)/I(G) corresponding to the transition between stage 1 and 2 shifts to higher disorder, i.e. lower L_a. Note also that I(D)/I(G)>0 even at UV excitation. (B) amorphisation trajectory for I(D)/I(G), showing the possibility of hysteresis.

The origin and dispersion of the D peak in disordered graphite arises from the double resonance mechanism corresponding to the k=0.5q condition of eq (1) [17-20,7]. In particular, symmetric breathing modes have the highest modulation of the polarizability and thus the highest Raman cross-section for k=0.5q [7]. Furthermore, there is a simultaneous mapping of the vibrational modes and electron energy levels of aromatic clusters onto those of graphite, according to the same k=0.5q condition. Aromatic clusters act as part of a graphite superlattice, both electronically and vibrationally [7]. Longer excitation wavelengths excite larger clusters with lower band gaps and lower frequency breathing modes. This is confirmed by calculations of Raman intensities of polycyclic aromatic hydrocarbons of increasing size, which exhibit two main bands corresponding to the G and D peaks in graphite [21,22]. As disorder increases, the I(D)/I(G) ratio disperses less. This means that the

D peak disappears for UV excitation in disordered and nanocrystalline graphite, but it is still present for amorphous carbons. In effect, for large disorder, as in sputtered a-C of Fig. 1(C), the D peak behaves like a non-dispersive vibrational density of states feature for the breathing modes of all ring-like sp^2 configurations. The presence of a residual D peak in UV Raman spectra of a-C's is a new finding, which can affect our deriving sp^3 content from the T peak, as discussed later.

Ideally, for an excitation energy E_{ex}, from (3) we expect clusters of size $L \propto 1/E_{ex}$ to give the largest contribution. Thus, for the highest E_{ex}, a-C with the smallest aromatic clusters will have the highest I(D)/I(G) with respect to nc-graphite. On the other hand the I(D)/I(G) ratio is bigger for bigger clusters, as shown by ab-initio calculations of Raman intensity [22], thus explaining the over-all decrease in I(D)/I(G) intensity for increasing excitation energy. Furthermore, very disordered amorphous carbons have a specific size distribution of clusters, and cannot span all the breathing mode frequencies of clusters of rings of arbitrary size, unlike in defected graphite, where all the upper optical branch is spanned by the double resonance condition for varying excitation energies. We therefore expect an almost constant I(D)/I(G) and D position for a-C. This is indeed seen experimentally, in Figs 2(B,C). In ta-C, there is no D peak at any wavelength, due to a complete absence of rings. These trends in I(D)/I(G) can be summarised by extending the three-stage model to many wavelengths, as in Fig 4(A). Note that the maximum of I(D)/I(G) versus L_a shifts to smaller L_a for increasing E_{ex}, as seen in Fig 4(A). Fig 4(B) shows the effect of hysteresis.

The T peak and sp^3 content

The first UV Raman studies [14,15] found a new peak at ~1060 cm^{-1} labelled T. This peak, seen only in UV excitation, is due to a resonant enhancement of the σ states, and it directly probes the sp^3 bonding. This peak corresponds to the peak in the CC sp^3 vibration density of states (VDOS) of ta-C in simulations [32,33] and EELS data [34]. Gilkes et al. [16] gave some empirical relations between the I(T)/I(G) ratio, the T peak position and the sp^3 content, Fig 2(D). Fig 5 compares the 244 nm UV Raman spectra of ta-C, ta-C:H, diamond-like a-C:H and polymeric a-C:H, with the peak fits adopted in this paper, to show the differences in their spectra in the T and D region.

The 244nm UV Raman spectra is a favoured means to derive the sp^3 content of amorphous carbons. This requires an understanding of how the spectrum develops with sp^3 content. For example, the variation of I(T)/I(G) with the sp^3 content is quite non-linear for 60 to 90% sp^3 contents, Fig 2(D1). The spectrum possesses the large G peak. If this is subtracted, this leaves the T peak, which arises from a peak in the sp^3 VDOS. As the sp^3 content falls, the sp^3 VDOS peak at 1060 cm^{-1} shifts upwards to that of a sp^2 network at 1400 cm^{-1} [34]. A shifting T feature is also seen in the UV Raman spectra of ta-C:N with increasing nitrogen content [35]. Alternatively, the changes could be represented as a reduction of the T peak at 1060 cm^{-1} and the rise of a peak around 1400 cm^{-1}, a D-like peak. This is consistent with the discussion in the previous section. There we noted that a small D peak can survive in UV in sp^2 a-C, where it becomes like a VDOS feature of sp^2 rings. Thus, as the sp^2 content of ta-C rises, the T peak intensity (corresponding to the CC sp^3 VDOS) is reduced, with a corresponding increase of a D peak. We use this model here.

A complication is that the D peak intensity depends not only on the sp^2 fraction, but also on its order. If the sp^2 sites have graphitic order, the D peak is absent in UV, if the sp^2 sites are in chains the D peak is absent, only if the sp^2 sites are in disordered rings does a residual D peak survive in UV.

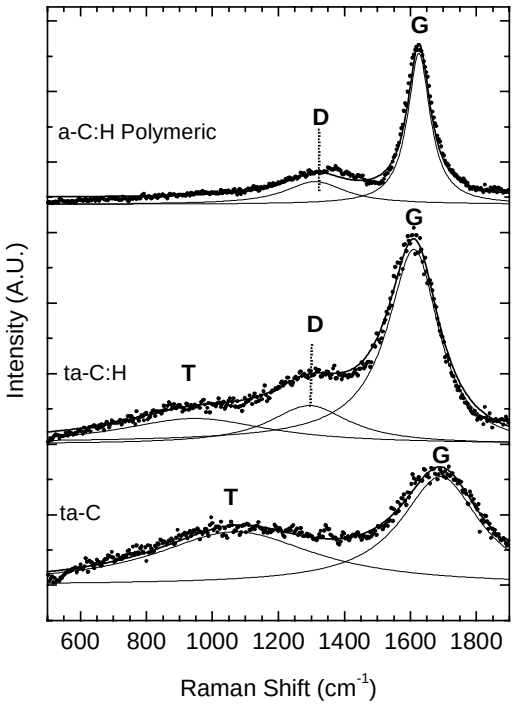

Fig 5: UV Raman spectra of polymeric a-C:H, ta-C:H and ta-C with the peak fits. The fitted peaks are correspondingly labelled. Note that for polymeric a-C:H a clear dip at ~1500 cm^{-1} exists between the D peak at the G peak. For ta-C:H (or diamond-like a-C:H) the residual D peak fills the dip around 1500 cm^{-1}.

This can then explain the range of I(T)/I(G) values seen for high sp^3 content ta-C. This could be attributed to the sensitivity of the T peak to small changes of sp^3 content at high sp^3 content. More likely, a slightly different amount of sp^2 clustering can fill in the dip around 1400 cm^{-1} so smearing the T peak intensity (clearly seen in the ta-C spectrum of Fig. 5). This could be overcome in principle by introducing an extra D peak in the fitting, even in samples with low sp^2 content, but a physically meaningful fit is difficult in these cases as this implies using two peaks to fit a broad feature with no clear modulations. Thus, the empirical relations of Gilkes et al. [16], obtained with a simple 2 peak fit (1 T peak and 1 G peak) that allows an up-shift of the T peak, are useful benchmarks.

The increase of sp^2 content and clustering both tend to reduce T peak intensity relative to the G peak. However, the T peak disappears only for large sp^2 contents. Thus, the effect of clustering is to reduce the direct correlation between T intensity and sp^3 content. Nevertheless, we can still distinguish high sp^3 contents from low sp^3, unlike in visible Raman spectra. Indeed, a T peak around 1060 cm^{-1} and an I(T)/I(G) ratio of about ~0.4-0.42 in H-free samples is a sufficient condition to estimate an sp^3 content of ~80%. An I(T)/I(G) ratio of 0.3-0.4 still indicates a sp^3 content of 60-80%, but sp^2 clustering makes it difficult to give a precise figure. Finally, I(T)/I(G)<0.2 indicates a sp^3 content lower than 20-30%. Thus the presence of a T peak is a powerful qualitative means to cut through the hysteresis. Indeed, a sample with high sp^3 fraction and large hysteresis will show a T peak (even if smaller than a similar sp^3 content sample, but with limited clustering of the sp^2 phase). On the other hand, a sample with low sp^3 fraction but with the same I(D)/I(G) in visible excitation will not show any T peak in the UV.

The analysis of T peaks extends to hydrogenated samples. Figs 1(B) shows that the T peak in ta-C:H or a-C:H is around ~980 cm^{-1}, lower than in ta-C. This is consistent with the

simulations of the C-C sp^3 VDOS in ta-C:H [36]. The presence of the residual D peak must be taken into account when fitting. As a first approximation, we use three Lorentzians to fit the spectra (Fig. 5). For hydrogenated samples, EELS gives the total amount of sp^3 bonded C atoms, in both C-C and C-H sp^3 bonds, but the T peak is sensitive only to C-C sp^3 bonds. Indeed, comparing the UV Raman spectra of ta-C:H and polymeric a-C:H (Figs 1(B) and 1(D)), it is clear that most C sp^3 atoms are bonded to H in polymeric a-C:H, due to the absence of a clear T peak, whilst in ta-C:H there is a sizeable amount of C-C sp^3 bonds. Empirically, I(T)/I(G)~0.1-0.2 in (t)a-C:H indicates an overall sp^3 content of ~70%. Further work is needed for more detailed conclusions. Clearly, as sp^2 clustering also contributes of a D peak, this can make things more difficult.

A final question for the I(T)/I(G) ratio in UV Raman is the cross-sectional uniformity of the sample. The samples here discussed are extremely uniform in the z direction [37]. However, it is possible to have quite layered ta-C films, with surface layers thicker than the penetration depth of UV light (~10-15 nm) [37]. In that case, UV Raman provides information on the outer part of the sample. On the other hand, this surface sensitivity can be exploited to investigate the changes induced by surface treatments.

CONCLUSIONS

We have presented the dispersion of Raman peaks with varying excitation energy for a comprehensive series of amorphous carbons. We showed how most trends can be classified and explained by extending the three-stage model developed to explain the visible Raman spectra of disordered and amorphous carbons.

We showed how amorphous carbons can have a D peak even in UV excitation, in contrast to disordered graphite. We discussed the origin of the trends of the T peak with sp^3 content for hydrogenated and hydrogen free samples. We showed how its blue-shift is due to the appearance of a residual D peak, due to the vibrations of all ring-like structures, and not to a change in the sp^3 VDOS, as sometimes suggested.

We also stress how the clustering of the sp^2 phase is the major parameter controlling the Raman spectra at any wavelength. Probing the same sample with visible and UV excitation allows us to derive the amount and clustering of sp^2 sites, at least qualitatively. This is due to the inversion of the trend of the G peak, resulting in a shift from visible to UV, which is larger for less sp^2 clustering. The appearance of the T peak gives a direct indication of the presence of sp^3 bonds. This means that a two wavelength study (eg at 514 nm and 244 nm) can provide a fast and powerful characterisation tool for amorphous and disordered carbons since the peaks' dispersion is a fingerprint which is specific to each different carbon system.

ACKNOWLEDGEMENTS

The author thanks John Robertson for guidance and fruitful discussions. The author acknowledges D. Batchelder of University of Leeds, M. Stutzmann of Walter Schottky Institut Muenchen, M. Kuball of University of Bristol, D. Richards of Cavendish Laboratory, Cambridge, G. Gibson of Materials Science and Metallurgy, Cambridge, and C. E. Bottani of Politecnico di Milano for the access to Raman facilities and kind hospitality in their laboratories and C. Castiglioni of Politecnico di Milano for useful discussions. Support from an European Union TMR Marie Curie fellowship and from Churchill College, Cambridge is gratefully acknowledged.

REFERENCES

1. J. Robertson, Prog. Solid State Chem **21**, 199 (1991); Pure Appl. Chem. **66**, 1789 (1994); J. Robertson, Adv. Phys., **35**, 317 (1986)
2. M. S. Dresselhaus, G. Dresselhaus, P. C. Eklund, *Science of Fullerenes and Carbon Nanotubes*, Academic Press, New York, 1996.
3. F. Tuinstra and J. L. Koening, J. Chem. Phys. **53**, 1126 (1970)
4. R. J. Nemanich, S. A. Solin, Phys. Rev. B, **20**, 329 (1979)
5. P. Lespade, A. Marchard, M. Couzi, F. Cruege, Carbon **22**, 375 (1984)
6. M. A. Tamor, W. C. Vassel, J. Appl. Phys. **76**, 3823 (1994)
7. A. C. Ferrari, J. Robertson, Phys. Rev. B, **61**, 14095 (2000)
8. A.M. Rao, E. Richter, S. Bandow, B. Chase, P. C. Eklund, K. A. Williams, S. Fang, K. R. Subbaswamy, M. Menon, A. Thess, R. E. Smalley, G. Dresselhaus, M. S. Dresselhaus, Science, **75**, 187 (1997)
9. D. S. Bethune, G. Meijer, W. C. Tang, H. J. Rosen, W. G. Golden, H. Seki, C. A. Brown, M. S. De Vries, Chem. Phys. Lett. **179**, 181 (1991)
10. S.D.M. Brown, P. Corio, A. Marucci, M. A. Pimenta, M. S. Dresselhaus, G. Dresselhaus, Phys. Rev. B, **61**, 7734 (2000)
11. S. D. M. Brown, P. Corio, A. Marucci, M. S. Dresselhaus, M. A. Pimenta, K. Kneipp, Phys. Rev. B, **61**, R5137 (2000)
12. A.C. Ferrari, J. Robertson, Phys. Rev. B, submitted (2000)
13. A.C. Ferrari, J. Robertson, Phys. Rev. B **63**, 121405(R) (2001).
14. K. W. K. Gilkes, H. S. Sands, D. N. Batchelder, J. Robertson, W. I. Milne, Appl. Phys. Lett. **70**, 1980 (1997)
15. V. I. Merkulov, J. S. Lannin, C. H. Munro, S. A. Asher, V. S. Veerasamy, W. I. Milne, Phys. Rev. Lett. **78**, 4869 (1997)
16. K. W. R. Gilkes, S. Prawer, K. W. Nugent, J. Robertson, H. S. Sands, Y. Lifshitz, X. Shi, J. Appl. Phys. **87**, 7283 (2000)
17. I. Pocsik, M. Hundhausen, M. Koos, L. Ley, J. Non-Cryst. Solids **227-230,** 1083 (1998)
18. M. J. Matthews, M. A. Pimenta, G. Dresselhaus, M. S. Dresselhaus, and M. Endo, Phys. Rev. B, **59**, 6585 (1999)
19. A.V. Baranov, A.N. Bekhterev, Y. S. Bobovich, V. I. Petrov, Opt. Spectrosc. **62**, 612 (1987)
20. C. Thomsen, S. Reich, Phys. Rev. Lett. **85**, 5214 (2000).
21. C. Mapelli, C. Castiglioni, G. Zerbi, K Mullen, Phys. Rev. B, **60**, 12710 (2000)
22. C. Castiglioni, C. Mapelli, F. Negri, and G. Zerbi, J. Chem. Phys. **114**, 963 (2001); M. Rigolo, C. Castiglioni, G. Zerbi and F. Negri, J. Mol. Structure, to be published (2001).
23. N.M.J. Conway, A.C. Ferrari, A. J. Flewitt, J. Robertson, W.I. Milne, A. Tagliaferro, W. Beyer, Diam. Relat. Mater. **9**, 765 (2000)
24. A. Ilie, A. C. Ferrari, T. Yagi, J. Robertson, Appl. Phys. Lett. **76**, 2627 (2000)
25. R. P. Vidano, D. B. Fishbach, L. J. Willis, T. M. Loehr, Solid. State Comm. **39**, 341 (1981)
26. P. Tan, Y. Deng, Q. Zhao, Phys. Rev. B, **58**, 5435 (1998)
27. Z. Wang, X. Huang, R. Xue, L. Chen, J. Appl. Phys. **84**, 227 (1998)
28. Y. Kawashima and G. Katagiri, Phys. Rev. B, **52**, 10053 (1995)
29. K. Sinha and J. Menendez, Phys. Rev. B **41**, 10845 (1990)
30. Y. Wang, D. C. Alsmeyer, R. L. McCreery, Chem. Mater. **2**, 557 (1990)
31. I. Pocsik, M. Koos, M. Hundhausen, L. Ley, in *Amorphous Carbon: State of the Art*, ed. by S. R. P. Silva et al. (Word Scientific, Singapore, 1998), p.224

32. T. Kohler, T. Frauenheim, G. Jungnickel, Phys. Rev. B **52**, 11837 (1995)
33. D. A. Drabold, P. A. Fedders and P. Strumm, Phys. Rev. B **49,** 16415 (1994)
34. G P Lopinski, V I Merkulov, J S Lannin, App Phys Lett 69 3348 (1996)
35. J. R. Shi, X. Shi, Z. Sun, E. Liu, B. K. Tay, S. P. Lau, Thin Solid Films **366**, 169 (2000)
36. F. Mauri, A. Del Corso, Appl. Phys. Lett. **75**, 644 (1999)
37. A.C. Ferrari, A. Libassi, B.K. Tanner, V. Stolojan, J. Yuan, L. M. Brown, S. E. Rodil, B. Kleinsorge, J. Robertson, Phys. Rev. B **62**, 11089 (2000)